Electronic Excitation Transfer from Carotenoid to Bacteriochlorophyll in the Purple Bacterium *Rhodopseudomonas acidophila*

Brent P. Krueger,[†] Gregory D. Scholes,[†,‡] Ralph Jimenez,[§] and Graham R. Fleming*[,†]

Department of Chemistry and The James Franck Institute, The University of Chicago, 5735 South Ellis Avenue, Chicago, Illinois 60637

Received: September 18, 1997; In Final Form: December 31, 1997

Ultrafast fluorescence upconversion has been used to probe electronic excitation transfer within the B800−B820 light-harvesting antenna of *Rhodopseudomonas acidophila* strain 7050. Emission from the carotenoid S_2 band decays in 54 ± 8 fs, and the bacteriochlorophyll B820 Q_y band rises in approximately 110 fs. The B820 Q_y rise time is wavelength-dependent. Energy-transfer rates between the carotenoid and several neighboring bacteriochlorophyll are calculated. Coupling strengths are estimated through transition dipole−transition dipole, polarization, and higher-order Coulombic coupling along with a new transition density volume coupling calculation. Data are compared to calculated energy-transfer rates through the use of a four-state model representing direct carotenoid to B820 energy transfer. The carotenoid emission data bound the S_2 to Q_x transfer time between 65 and 130 fs. The S_1 to Q_y transfer is assumed to be mediated by polarization and Coulombic coupling rather than by exchange; the transfer time is estimated to be in the picosecond regime, consistent with fluorescence quantum yield data.

I. Introduction

Photosynthesis in plants and some bacteria involves a series of extremely efficient steps that convert light energy into chemical energy. Both plants and bacteria have evolved systems in which a large number of chromophores act as light-harvesting antenna to direct solar energy to a single reaction center, where the charge separation that drives the chemistry of photosynthesis occurs.[1−3] In purple photosynthetic bacteria, there are, generally, two types of light-harvesting antenna complexes—LH1 (core) and LH2 (peripheral)—each of which contains dozens of chromophores. A single LH1 complex is thought to be closely associated with a single reaction center, while several LH2 complexes are thought to associate with a single LH1/reaction center unit.[4,5] The recent high-resolution crystal structures of the LH2 of *Rhodospirillum molischianum*[6] and *Rhodopseudomonas (Rps.) acidophila*[7] reveal 8-fold and 9-fold symmetric ring structures, respectively, and close interactions between bacteriochlorophyll (Bchl) and carotenoid molecules, the two different chromophores in the system.[8−10]

In this paper, we address some of the issues surrounding the carotenoid−Bchl interactions. We present fluorescence upconversion data which show rapid decay in carotenoid excited-state population and rise in Bchl excited-state population. We use several methods to estimate coupling strengths between the relevant transitions including a new method that makes use of molecular transition density volumes rather than simple transition dipoles. Also, we determine the relevant spectral overlaps and use these along with the coupling strengths to estimate energy-transfer rates between the carotenoid and Bchl. These rates are compared to the fluorescence upconversion data and are discussed in terms of possible mechanisms of energy transfer from carotenoid to Bchl.

First we provide a brief introduction to the behavior and function of carotenoids in bacterial light-harvesting antenna. The role of carotenoids within light-harvesting complexes is 3-fold.[11,12] They provide structural stabilization for the complex, provide photoprotection by quenching excess triplet and in some circumstances singlet energy from (bacterio)chlorophyll, and, particularly in purple bacteria, perform a vital light-harvesting function.

In purple bacteria, carotenoids are light harvesters that quickly and efficiently transfer singlet energy to neighboring Bchl. Figure 1 shows the important singlet states of the carotenoid and B820 Bchl molecules along with two possible routes of energy transfer. Both the Q_x and Q_y states of the Bchl are associated with strongly absorbing transitions from the ground state. The properties of the carotenoid singlet states are more complex.

In analogy to the closely related all-trans polyenes of C_{2h} symmetry (see Scheme 1 of section IVB for the chemical structures of two carotenoids), the lowest excited carotenoid singlet state, S_1, is labeled $2\ ^1A_g$, and the transition from the ground state (S_0, $1\ ^1A_g$) is optically "forbidden". The next carotenoid singlet state, S_2, is labeled $1\ ^1B_u$ and is a strongly allowed optical transition from the ground state. The well-characterized $S_2 \leftarrow S_0$ transition exhibits a broad vibronic structure peaked near 490 nm (20 400 cm^{-1}) for in situ rhodopin glucoside—the carotenoid present in *Rps. acidophila*. The position of the S_1 state is less well-known. A variety of techniques have been used to provide estimates of the energetic position of the S_1 state for several carotenoids.[12−17] However, appropriate experimental data do not yet exist for rhodopin glucoside. We will address this point further in section IVB.

[†] Present address: Department of Chemistry, The University of California at Berkeley, Berkeley, CA 94720-1460. E-mail: fleming@cchem.berkeley.edu.

[‡] Department of Chemistry, Imperial College of Science, Technology and Medicine, Exhibition Road, London SW7 2AY, United Kingdom.

[§] Present address: Department of Chemistry and Biochemistry, The University of California, San Diego, 9500 Gilman Drive Mailstop 0339, La Jolla, CA 92093-0339. E-mail: rxj@chem.ucsd.edu.

S1089-5647(97)03062-9 CCC: $15.00
Published on Web 02/27/1998

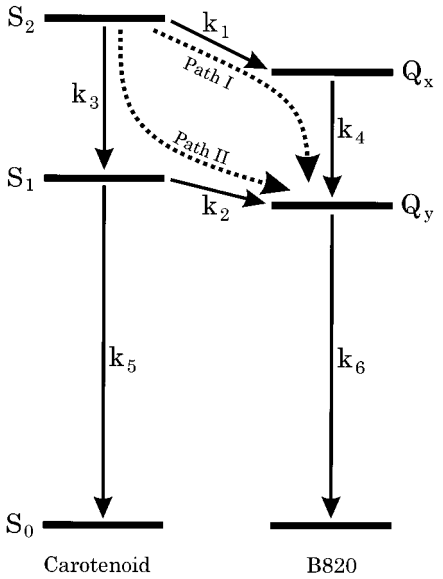

Figure 1. Scheme of energy-transfer and relaxation processes involving the carotenoid and Bchl B820.

Because the "forbidden" $S_1 \rightarrow S_0$ transition is lower in energy than the allowed $S_2 \rightarrow S_0$ transition, carotenoids exhibit unusual optical properties. Lack of emission from the $S_1 \rightarrow S_0$ transition and rapid internal conversion from the S_2 state to the S_1 state result in weak emission from carotenoids; population moves from "bright" S_2 to "dark" S_1 before S_2 can emit. This behavior would suggest that carotenoids make poor energy donors for energy transfer and thus poor light-harvesting pigments. Electronic excitation transfer (EET) from the carotenoid S_2 state to the Bchl Q_x state (path I) must compete against the extremely rapid $S_2 \rightarrow S_1$ internal conversion which occurs on a time scale of a few hundred femtoseconds.[18−22]

Additionally, the forbidden nature of the $S_1 \leftarrow S_0$ transition implies that there is no dipole−dipole coupling between the carotenoid $S_1 \rightarrow S_0$ transition and the Bchl $Q_y \leftarrow S_0$ transition, and therefore, the rate of Förster-type[23] transfer is zero. It was originally believed (see ref 24 for an early review) that excitation energy placed in the carotenoid S_2 state internally converted to the carotenoid S_1 state before S_2 to Q_x transfer could occur. From the longer lived S_1 state, energy could be transferred to the Bchl molecule via an exchange type[25] of coupling. However, transient absorption measurements on *Chromatium (C.) purpuratum*[22] and *Rhodobacter (Rb.) sphaeroides*[18,20] have suggested that carotenoid S_2 to Bchl Q_x transfer is competitive with carotenoid S_2-S_1 internal conversion. As mentioned earlier, it has generally been assumed that an exchange type of coupling[25] was responsible for carotenoid S_1-Bchl Q_y (path II) EET, but recently it has been shown that, even at the small separations present in light-harvesting complexes, higher order Coulombic terms and polarization interactions are likely to dominate over exchange terms.[26,27]

The possibility of rapid carotenoid to Bchl energy transfer is supported by the small chromophore separations revealed by the crystallographic data. Analysis of the data indicates that portions of the carotenoid lie within 6 Å of the central Mg of the B820 Bchl and significantly closer to several of the B820 Bchl carbon atoms.[7,10] (Note that *Rps. acidophila* naturally makes several types of LH2 depending on the particular strain and growth conditions.[28] One of these is the B800−B850 complex described by the crystallographic data; another is the B800−B820 complex used in this study. In the former, one-third of the Bchl absorb at 800 nm (B800 Bchl) and two-thirds at 850 nm (B850 Bchl). In the latter, the B850 Bchl absorption is blue-shifted, resulting in Bchl that absorb at 820 nm, B820. There are several detailed structural studies of the B800−B850 complex, and we assume that those descriptions are also representative of the B800−B820 complex, as suggested by significant sequence homology between the respective proteins.[29,30] A more complete description of light harvesting in photosynthesis is given in ref 3.) This proximity suggests that there may be a strong coupling between the transition moments, promoting rapid (<200 fs) energy transfer from the carotenoid S_2 state to the Bchl Q_x state (path I of Figure 1). In addition, the rapid transfer rates in this system suggest that donor species are not vibrationally relaxed prior to EET and that time-dependent spectral overlap integrals may need to be considered.[31]

Recent experimental work using transient absorption measurements has begun to assign energy-transfer rates to some of the many possible energy-transfer pathways present in LH2. Shreve et al. and Trautman et al. studied *Rb. sphaeroides* B800−B850 complexes; they have suggested a carotenoid−B850 transfer time of 200 fs,[18] carotenoid S_2-Bchl B800 transfer time of 1.7 ps, carotenoid S_1-Bchl B800 transfer time of 3.8 ps, and B800−B850 transfer time of 700 fs.[20] Andersson et al. studied *C. purpuratum* B800−B830 complexes and have suggested two separate carotenoids, one which is coupled to B830 and the other to B800. Carotenoid1 transfers S_2-B830 Q_x in 50−100 fs and S_1-B830 Q_y in 3.8 ps. Carotenoid2 does not transfer S_2-B800 Q_x and transfers S_1-B800 Q_y in 490 fs.[22] Fluorescence upconversion data from the B800−B850 LH2 complexes of *Rps. acidophila* have also been reported.[32] These data are modeled by 100 fs carotenoid S_2-Bchl B850 Q_x transfer and 3 ps carotenoid S_1-Bchl B850 Q_y transfer and are generally consistent with the transient absorption work cited above.

In this work, we use fluorescence upconversion experiments to investigate the EET from the carotenoid to the B820 Bchl of B800−B820 LH2 complexes from *Rps. acidophila*. Both experimental and calculated estimates of energy-transfer rates are discussed in terms of the possible carotenoid−Bchl coupling mechanisms involved. The context for energy transfer is given by the four-state model involving the lowest two excited singlet states of the carotenoid and B820 Bchl molecules (Figure 1).

II. Experimental Section

The samples used for this work were generously provided by R. van Grondelle. B800−B820 complexes were isolated from *Rps. acidophila* strain 7050 and solubilized in the detergent *n*-dodecylmaltoside. Details of the preparation are as given by Angerhofer and co-workers,[33] except for the use of *n*-dodecylmaltoside in place of LDAO.

Fluorescence upconversion experiments have been described previously.[34,35] Briefly, a tunable, mode-locked, titanium: sapphire laser (Coherent Mira 900F with long wavelength mirror set) provided a 76 MHz pulse train of 980 nm light which was doubled in a 1 mm LBO crystal (CSK). The resulting 490 nm second harmonic formed the excitation beam, while the residual IR served as the gate beam. The excitation pulses were focused into a 1 mm path length quartz sample cell placed at one focus of an elliptical reflector. The spontaneous emission from the sample was collected by the elliptical reflector and focused into the upconversion crystal (0.5 mm BBO) placed at the other focus of the ellipse. Mixing of the emission and the gate beam in the upconversion crystal yielded ∼8 nm bandwidth up-converted emission which was collimated with a lens. A prism and double monochromator were used to select the desired spectral region with ∼6 nm of bandwidth which was detected by a photomultiplier tube.

All experiments detected isotropic emission by passing the gate and excitation beams through polarizers (1 cm calcite) oriented at the magic angle relative to each other. Excitation pulse energy was ~0.5 nJ. The ~4 mL of sample was flowed with a peristaltic pump while being cooled in an ice water bath.

Fitting was performed by convolution of a model decay curve with an instrument response function and iterative comparison to data using a nonlinear least-squares algorithm. The instrument response function (IRF) was approximated by cross-correlating the gate and excitation beams while flowing a detergent solution through the sample cell. A typical IRF exhibited a 160 fs full width at half-maximum (fwhm) and was well described by a Gaussian form, implying a Gaussian excitation pulse with a fwhm of 110 fs.

Four data sets are utilized in this paper. Excitation was at 490 nm (the carotenoid $S_2 \leftarrow S_0$ transition) for all sets. Emission was detected at 550 nm (peak of carotenoid emission), 830 nm, 840 nm (peak of B820 emission), and 850 nm. Acquisition times were 2 h for 550 nm data (scanned from −500 fs to 1 ps) and from 30 to 50 h for each of the other three sets (scanned from −750 fs to 10 ps). Instrument response functions taken before and after each data set and constant monitoring of the laser spectrum verified laser stability over the data acquisition period. Absorption spectra taken throughout data acquisition demonstrated some sample degradation during the three long Bchl emission wavelength sets. The shape of the spectrum assigned to each chromophore was unchanged throughout the experiment, though the absorption of the carotenoid peaks steadily reduced relative to the constant Bchl peaks. However, because signal in these data sets is obtained only after a successful EET event, this degradation should result only in a reduced signal level.

Steady-state absorption and emission spectra were taken in a 1 mm path length quartz cuvette with the same concentrations used for the time-resolved data. Absorption spectra were taken on a Shimadzu UV-1601 spectrophotometer. Emission spectra were taken on a SPEX fluorolog-2 fluorometer in the front-face geometry (which eliminates any aberrations due to self-absorption) and corrected for detector sensitivity (via correction factors determined by previous comparison to a NIST-traceable lamp spectrum).

III. Results

Steady-state absorption and emission spectra of the B800−B820 complex are given by the dotted and solid lines, respectively, of Figure 2. They are typical for this system,[33] though it is notable that carotenoid emission is apparent in the 500−600 nm region shown by the inset. Poor signal-to-noise precludes careful analysis of the emission in the carotenoid region though it does suggest a mirror-image vibronic profile.

Figure 3 shows upconversion data and a fit for emission from the carotenoid S_2 state (550 nm) of the B800−B820 complex which was excited into the carotenoid S_2 state (490 nm). The data are best fit to a function with a biexponential decay with time constants (amplitudes) of 54 ± 8 fs (98%) and 250 fs (2%). The 54 fs component is attributed to the in situ lifetime of the S_2 state of the carotenoid. The longer component is similar to the solution lifetime[21] and may be due to a subpopulation of carotenoids that are either adjacent to a triplet excited Bchl molecule (the high repetition rate of the laser produces a significant steady-state population of triplet Bchl[36]) or due to carotenoids that are not connected to a Bchl (e.g., attached to denatured protein or free in detergent solution).

Figure 4 shows upconversion data and fits for Bchl Q_y emission at 830, 840, and 850 nm following excitation into the carotenoid S_2 state. All three are fit to a function with a single-exponential rise and a biexponential decay. The signal-to-noise is inadequate in any of the sets to determine confidently additional rise or decay components. The blue edge emission (830 nm) gives fit parameters with a 90 ± 50 fs rise of 100% and decays of 1.0 ± 0.3 ps (25%) and 16 ± 2 ps (75%). The fit to the data from the peak of emission (840 nm) yields fit parameters with a 110 ± 25 fs rise of 95% and decays of 2.7 ± 0.4 ps (40%) and >40 ps (60%). The emission from the red edge of the band (850 nm) gives fit parameters with a 150 ± 60 fs rise of 120% and decays of 4.0 ± 0.8 ps (55%) and >100 ps (45%). Because of spectral evolution during the first 1−2 ps and poor signal-to-noise, we hesitate to assign these individual decay components; however, it is likely that each fit should contain a rapid rise attributable to EET from the initially excited carotenoid S_2 state by some pathway in Figure 1, along with a multicomponent decay that can be assigned to singlet−singlet or singlet−triplet annihilation,[36] in addition to intraband dynamics. Despite rather large uncertainties in the decay components, overlaying the three Bchl emission profiles and close examina-

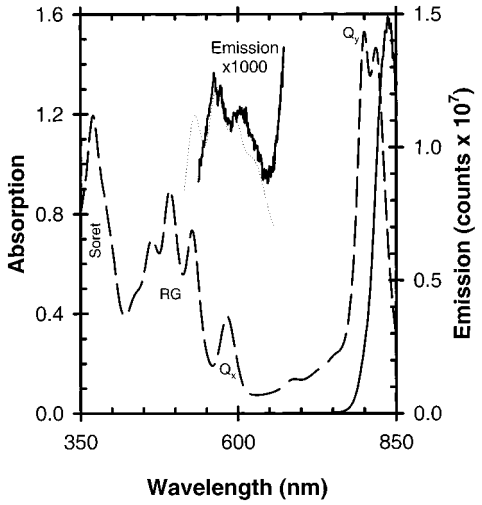

Figure 2. Steady-state absorption (dashed) and emission (solid) spectra from B800−B820 complexes of *Rps. acidophila*. In the absorption spectrum, the Bchl Soret peak is labeled Soret; the four carotenoid peaks, RG; the Bchl Q_x peak, Q_x; and the 800 and 820 nm Bchl Q_y peaks, Q_y. The inset expands the emission spectrum (solid) in the region of the carotenoid emission and shows the representation of the S_2 emission (dotted) used in this work (parameters given in Table 2).

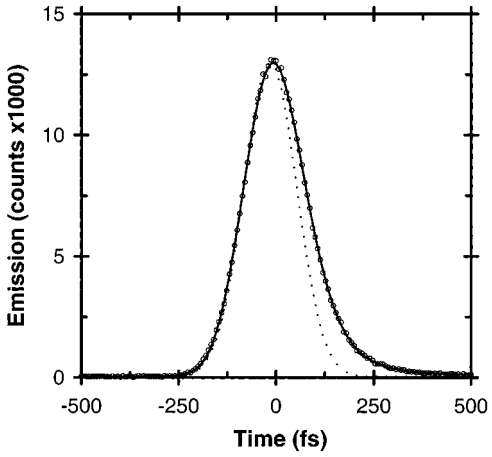

Figure 3. Upconversion data from the carotenoid S_2 emission detected at 550 nm. Excitation was at 490 nm and the scan range was −500 fs to 1 ps. Open circles represent the data, the dotted line is the instrument response function, and the solid line is a biexponential fit: 54 ± 8 fs (98%) and 250 fs (2%).

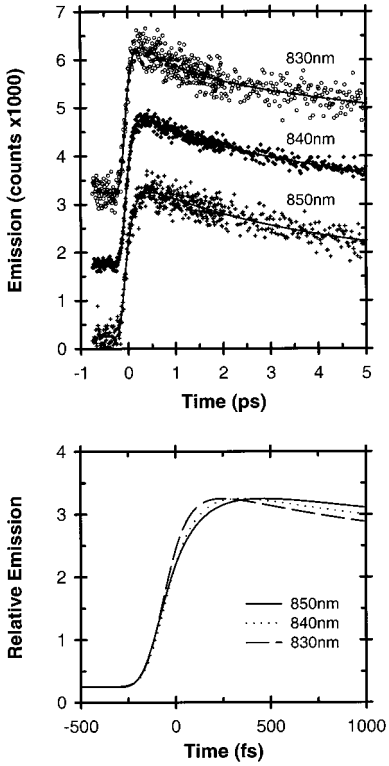

Figure 4. (top) Upconversion data from the Bchl Q_y detected at 830, 840, and 850 nm. Excitation was at 490 nm, and the scan range was −750 fs to 10 ps for all sets. The solid line represents the fit for each data set with parameters as given in section III of the text. The data sets (○, 830 nm; ◆, 840 nm; +, 850 nm) are each separated by 1500 counts of vertical offset. (bottom) The same three fits to the Bchl Q_y data sets shown above, normalized to the same maximum counts and overlayed.

tion of Figure 4 reveals that the rise times and decay shapes of the three profiles are significantly different. These differences between the high- and low-energy (short- and long-wavelength) sides of the emission can be attributed to the several thousand wavenumbers of cooling that must occur within the Q_y band after EET from the higher energy donor state.

The presence of vibrational cooling within the Q_y band emission profiles makes any single emission curve a poor representative of band dynamics. Wavelength-dependent emission profiles were also observed in *Rb. sphaeroides* and made the extraction of energy-transfer times ambiguous.[37] The significant differences between the three curves of Figure 4 show that intraband (e.g., vibrational cooling) dynamics are strongly convoluted with internal conversion and energy-transfer dynamics in this system. Of particular interest is the variation in rise times from 90 to 110 to 150 fs when moving from 830 to 840 to 850 nm. Ideally, we should construct a time-resolved B820 Q_y band emission spectrum. However, at present, we do not have enough data to accurately assemble a single curve, especially in the critical early time period. Therefore, we have used the 840 nm emission data to estimate the time-dependent Q_y state population.

IV. Discussion

A. Four-State Model. We will interpret the time constants of the upconversion data in the context of the four-state model shown in Figure 1. The energy level diagram gives approximate positions of the ground and first two excited singlet states of the carotenoid and B820 Bchl. (Note that the energy of the carotenoid S_1 state is unknown. We estimate its energy in section IVB.) Carotenoid to Bchl EET rates are given by k_1 for S_2 to Q_x and by k_2 for S_1 to Q_y. The S_2 to S_1 and Q_x to Q_y internal conversion rates are given by k_3 and k_4, respectively. The total rates of depopulation of the S_1 and Q_y states are represented by k_5 and k_6, respectively. With the assumption that the initial population of state S_2 is unity and that each of the other states is zero, we obtain the following expressions for the populations, $P(t)$, of the S_2 and Q_y states:

$$P_{S_2}(t) = e^{-(k_1+k_3)t} \quad (1)$$

$$P_{Q_y}(t) = C_1 e^{-(k_1+k_3)t} + C_2 e^{-k_4 t} + C_3 e^{-(k_2+k_5)t} + C_4 e^{-k_6 t} \quad (2)$$

where

$$C_1 = \frac{k_2k_3(k_1 + k_3 - k_4) + k_1k_4(k_1 - k_2 + k_3 - k_5)}{(k_1 + k_3 - k_4)(k_1 - k_2 + k_3 - k_5)(k_1 + k_3 - k_6)}$$

$$C_2 = \frac{-k_1k_4}{(k_1 + k_3 - k_4)(k_4 - k_6)}$$

$$C_3 = \frac{-k_2k_3}{(k_1 - k_2 + k_3 - k_5)(k_2 + k_5 - k_6)}$$

$$C_4 = -(C_1 + C_2 + C_3)$$

The population decay rate of the carotenoid S_2 state (eq 1) is given by the sum of k_1 and k_3. Therefore, selecting a reasonable value for k_3 allows calculation of k_1 given the measured lifetime of 54 ± 8 fs. Recent measurements of the S_2 lifetime of rhodopin glucoside in benzyl alcohol solution suggest a value for k_3^{-1} of 135 fs,[38] which leads to an estimate for k_1^{-1} (S_2-Q_x EET) of 90^{+25}_{-20} fs. However, twisting of the carotenoid by the surrounding protein in situ[7] may change k_3 significantly from estimates based on solution spectroscopy.[21,39] Representing k_3^{-1} by the more conservative range of 120−150 fs leads to a bracketing of k_1^{-1} between 65 and 130 fs.

We can now address k_4, k_5, and k_6. Recent measurements on internal conversion rates in Bchl have bracketed k_4^{-1} between 100 and 400 fs,[40] while earlier measurements in reaction centers suggest a range of 150−250 fs;[41] we use 200 fs. Applying the energy gap law[42−44] to the extrapolation of the rhodopin glucoside S_1 energy of section B yields an S_1-S_0 internal conversion time of k_5^{-1} = 3.5 ps. Transient absorption measurements at 820 nm provide a reasonable estimate for k_6^{-1} of 800 ps.[45]

As mentioned earlier, the high repetition rate of the laser brings annihilation dynamics into play. Also, the use of the 840 nm emission to represent the Q_y state population results in intraband dynamics, not accounted for in the model, being present in the data. Therefore, we put two additional exponential decays into eq 2: one to account for annihilation and the other for vibrational cooling.

$$\mathrm{FIT}_{Q_y}(t) = P_{Q_y}(t)((1 - A_{IB} - A_{An}) + A_{IB}e^{-k_{IB}t} + A_{An}e^{-k_{An}t}) \quad (3)$$

A_{IB} and A_{An} are the amplitudes of intraband and annihilation decays; k_{IB} and k_{An} are the rates of intraband and annihilation decays. We then fit the data with the six rates of the four-state model fixed, while allowing the amplitude and decay time of the two additional components to be determined by the fitting program. Three different fits were found; in each we chose a

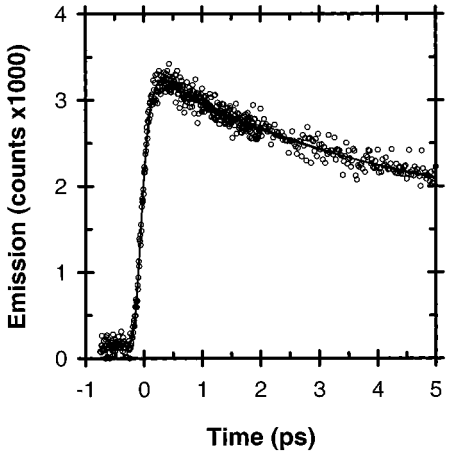

Figure 5. The 840 nm emission (open circles), representing the full Q_y band population, and fits. The three indistinguishable fits, with parameters given in Table 1, are given by the solid line.

TABLE 1: Parameters Obtained from Three Separate Fits of the Four-State Model Described in the Text to the 840 nm Emission[a]

fit	k_1^{-1} (fs)[b]	k_2^{-1} (ps)[b]	k_3^{-1} (fs)[b]	k_4^{-1} (fs)[b]	k_5^{-1} (ps)[b]	k_6^{-1} (ps)[b]	IB Amp	IB Dec (fs)	An Amp	An Dec (ps)
1	90	1.0	135	200	3.5	800	0.59	300	0.23	3.2
2	90	14	135	200	3.5	800	0.57	220	0.25	3.5
3	90	100	135	200	3.5	800	0.58	210	0.23	3.9

[a] k_1-k_6 are defined in Figure 1 while An Amp and An Dec refer to the amplitude (fraction) and decay time of annihilation kinetics included in the fit. Similarly, IB Amp and IB Dec refer to the amplitude (fraction) and time scale of the intraband dynamics included in the fit. [b] These parameters were fixed at these values.

different value for k_2, the S_1 to Q_y rate. The three resulting fits are indistinguishable and are seen as a single line, along with open circles representing the emission curve, in Figure 5. Parameters for the fits are given in Table 1.

It is clear that fitting the emission curve to the four-state model does not allow us to limit the possible value of k_2. Curves generated directly from eq 2, lacking annihilation and vibrational relaxation, do differ significantly from each other in the picosecond regime. However, because the annihilation kinetics occur on the same time scale as the crucial portion of the dynamics, we are unable to use our emission decays to differentiate between possible values of k_2.

As an alternative to directly fitting the time-resolved data to determine k_2, we can use the above rates along with bounds on the total carotenoid to Bchl transfer efficiency determined from steady-state data[33] to estimate k_2. Using the measured lifetime of the S_2 state of 54 ± 8 fs and assuming that the lifetime of the S_1 state is 3.5 ps, that the S_2-S_1 internal conversion time ranges between 120 and 150 fs, and that the overall carotenoid to Bchl efficiency is the maximum allowed by steady-state measurements (75%[33]) yields S_1-Q_y transfer times that range from 3 to 15 ps. This calculation suggests that S_2-Q_x transfer (path I) accounts for 48−70% of the S_2 excitation reaching the Q_y state and that from 27% to 5% of the S_2 excitation must reach the Q_y state via path II, while the remaining 25% reaches the carotenoid ground state.

B. Spectral Overlap. Following Förster,[23] we will use the following general expression for the rate of EET (using D and A to represent donor and acceptor):

$$k = (4\pi^2/h^2c)|T_{DA}|^2 J \qquad (4)$$

TABLE 2: Parameters for Absorption (Top) and Emission (Bottom) Line Shapes Used for the Calculation of Spectral Overlaps[a]

species	Gaussian center (cm^{-1})	Gaussian width (cm^{-1})	Amp ($\times 10^{-4}$ cm)
carotenoid S_2 Abs	18 940	1040	2.916
carotenoid S_2 Abs	20 260	1050	2.904
carotenoid S_2 Abs	21 530	1330	1.713
carotenoid S_2 Abs	22 870	1320	0.661
carotenoid S_2 Abs[b]	24 180	1470	0.112
Bchl Q_x	17 160	300	31.31
Bchl B800 Q_y	12 540	200	46.97
Bchl B820 Q_y	12 170	200	46.97
S_2 emission (S_1)	17 740 (12 000)	1040	2.916
S_2 emission (S_1)	16 430 (10 690)	1050	2.904
S_2 emission (S_1)	15 150 (9410)	1330	1.713
S_2 emission (S_1)	13 820 (8070)	1320	0.661
S_2 emission (S_1)[b]	12 510 (6770)	1470	0.112

[a] The amplitudes are given such that the integrated spectral area of each species, on a wavenumber scale, is unity. [b] The last carotenoid vibronic peak is extrapolated from the first four.

where T_{DA} is the coupling term (in wavenumbers). The spectral overlap integral, J, is given by

$$J = \int\left[\int g'(E')\, S_D{}^2(E',E'-h\nu)\, dE'\right] \times \left[\int g(E)\, S_A{}^2(E,E+h\nu)\, dE\right] d\nu \qquad (5)$$

in which g and g' are Boltzmann factors and S_D and S_A are pure vibrational overlap integrals.[23] The terms in the square brackets can be related to the emission and absorption spectra, resulting in

$$J = \int G'_D(\nu)\, G_A(\nu)\, d\nu \qquad (6)$$

where

$$G_A(\nu) \equiv A\frac{\epsilon_A(\nu)}{\nu} = \int g S_A{}^2\, dE$$

$$G'_D(\nu) \equiv B\frac{f_D(\nu)}{\nu^3} = \int g' S_D{}^2\, dE'$$

The integrals on the right are shorthand for the integrals in square brackets of eq 5. ϵ_A and f_D are the acceptor absorption spectrum and donor emission spectrum, respectively. The constants A and B are chosen such that the line shape functions, G_A and G'_D, are each normalized to unit area on a wavenumber (ν) scale.

The absorption spectrum (Figure 2) is converted into the absorption line shape, G_A, and fit to several Gaussians, each of which is assigned to a particular transition (i.e., S_2, Q_x, and Q_y of B800 and B820). Figure 2 shows that four carotenoid vibronic peaks are visible in the absorption spectrum; any additional peaks are obscured by the presence of the Bchl Soret bands. We use Franck−Condon and Boltzmann factors to estimate the amplitude of a fifth vibronic peak (assuming two displaced, harmonic oscillators with parameters chosen to fit the relative amplitudes of the four visible peaks) and find that it is roughly 20% of the fourth peak. The amplitude of a sixth vibronic peak is negligible. Parameters for this representation of the S_2 absorption spectrum are given in Table 2.

The various Bchl absorption line shapes are each represented by a single Gaussian. For accurate calculation of the spectral overlap, the width of the profile must be representative of the

SCHEME 1

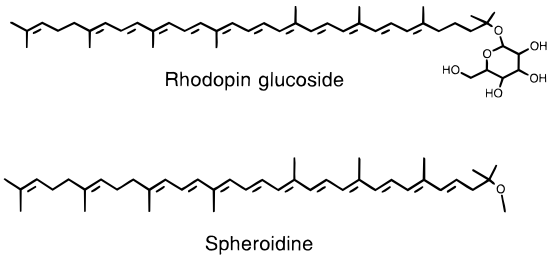

homogeneous line width. Joo et al. used photon echo experiments[46] to determine the homogeneous line width of B800 in *Rb. sphaeroides* LH2 to be 200 cm^{-1} whereas Sauer et al. used a value of 300 cm^{-1} for the homogeneous line width of B800 and B850 in recent calculations of LH2 optical spectra.[47] We use the 200 cm^{-1} value for our Q_y absorption profiles, but sample calculations using 300 cm^{-1} result in only a small (<5%) increase in the value of the overlap. The homogeneous line width for the Q_x band is less well-known. We estimate a width of 300 cm^{-1} for our calculations of spectral overlap, but again, widths ranging from 200 to 870 cm^{-1} (width of the steady-state line shape peak) result in <10% change in the spectral overlap due, partially, to the positioning of the Q_x band midway between two of the carotenoid S_2 emission peaks. Final parameters for all acceptor absorption line shapes are given in Table 2.

The donor emission line shape for the carotenoid S_2 state can be taken from the S_2 absorption line shape. Spectral studies of carotenoids indicate that the S_2 emission closely mirrors the S_2 absorption.[16,21] Therefore, to obtain the S_2 emission line shape, we mirror the absorption and red shift it until it overlaps the small peak visible in the steady-state emission of the B800−B820 complex around 570 nm (see Figure 2). This red shift represents a Stokes shift of 1200 cm^{-1} (528−563 nm), similar to values displayed by other systems of this type.[20,21] Normalizing the line shape to unit area gives the final parameters for the S_2 donor emission line shape which are given in the lower portion of Table 2.

Estimating the line shape of the S_1 donor emission involves considerable approximation. Several intermediate length polyenes and carotenoids emit from both the S_1 and S_2 states.[16,48] In these systems, the two states show roughly similar spectral shapes though, as pointed out by Chynwatt and Frank,[15] the S_1 emission tends to peak one vibronic band to the red of the S_2 emission peak. However, in the absence of definite spectral data, applying the S_2 spectral profile to S_1 provides a reasonable starting place. The S_2 emission line shape found above is simply red-shifted so that its highest energy (0−0) vibronic peak coincides with the S_1 energy estimated below.

Several groups have used spheroidene analogues containing 7, 8, and 9 conjugated double bonds, in which both the S_1 and S_2 states can be observed, to estimate the S_1 energy of spheroidene, containing 10 conjugated double bonds, in which the S_1 state is unobservable.[14−16] By extending this extrapolation to 11 conjugated double bonds, the S_1 energy of rhodopin glucoside can be estimated.

Scheme 1 shows that, aside from the positioning of the saturated bonds, the polyene backbone is identical in the two carotenoids.[49] Thus, extending the work on spheroidene to 11 double bonds leads to a reasonable estimate of ∼13 000 cm^{-1} as the energy of the S_1 state of rhodopin glucoside.

To properly position the S_1 emission profile, we also need an estimate for the Stokes shift. Presumably, the S_2 Stokes shift is primarily determined by intramolecular contributions, although the S_2 state sensitivity to solvent polarizability[50] suggests that there should also be a significant component of the Stokes shift due to solvation effects. For the S_1 state, the energy gap is fairly independent of solvent, so the solvent contribution should be minimal; however, little is known about the intramolecular contribution to the S_1 Stokes shift. For lack of detailed information we, rather arbitrarily, estimate a value of 1000 cm^{-1} for the S_1 Stokes shift which places the 0−0 band of the S_1 emission at 12 000 cm^{-1}. Final parameters for the S_1 donor emission line shape, with amplitudes determined by unit normalization, are given in Table 2. With spectral line shapes for all relevant species, spectral overlaps are easily calculated using eq 6 and the line shapes given in Table 2. Final values for the relevant spectral overlaps are given in Table 3.

TABLE 3: Values of *J*, the Spectral Overlap Integral of Bchl Acceptors with Carotenoid Donors[a]

acceptor	S_2 emission (cm)	S_1 emission (cm)
Bchl Q_x	2.06×10^{-4}	1.58×10^{-31}
Bchl B800 Q_y	1.62×10^{-5}	1.41×10^{-4}
Bchl B820 Q_y	1.06×10^{-5}	2.68×10^{-4}

[a] Values are calculated using eq 6 with the line shapes defined by the parameters in Table 2.

C. Couplings and Rates. We now complete calculation-based estimation of k_1 and k_2 by estimating coupling strengths between the various states. We use Förster theory to estimate S_2-Q_x coupling, while to estimate the S_1-Q_y coupling, we make use of more sophisticated techniques described by Scholes al.[27] which are discussed briefly below. In addition, we present preliminary results from calculations that avoid the difficulties of the point Coulombic expansion used in Förster theory to estimate the S_2-Q_x coupling by using transition density volumes of the donor and acceptor. These coupling strengths are used in eq 4 along with the spectral overlaps to estimate the transfer rates.

We begin by estimating the rate for the S_2 to Q_x EET, k_1. Within the point dipole approximation, the coupling term associated with k_1 corresponds to the standard transition dipole−transition dipole interaction given by Förster.[23] We write the coupling as

$$|T_{DA}| = 5042 \frac{\kappa|\mu_D||\mu_A|}{n^2 R_{DA}{}^3} \tag{7}$$

where T_{DA} is in wavenumbers, μ_D and μ_A are the transition dipole moments of the donor and acceptor in debyes, n is the index of refraction of the surrounding medium (unitless), and R_{DA} is the distance between the centers of the dipoles in angstroms. The orientational factor, κ, is determined by

$$\kappa = \mathbf{u}_D \cdot \mathbf{u}_A - 3(\mathbf{u}_D \cdot \mathbf{r}_{DA})(\mathbf{u}_A \cdot \mathbf{r}_{DA}) \tag{8}$$

where $\mathbf{u}_D$ and $\mathbf{u}_A$ are unit vectors in the directions of the transition dipole moments and $\mathbf{r}_{DA}$ is the unit vector along the line connecting the centers of the two chromophores. The unit vectors are taken from the crystal structure[7] where the $\mathbf{u}$ for the carotenoid is taken as the average of unit vectors placed along each of the conjugated bonds. The $\mathbf{u}$ for each of the Bchl transitions is taken to be along the vector connecting the appropriate nitrogen atom pair. Table 4 gives values of κ for the carotenoid $S_2 \rightarrow S_0$ transition as $\mathbf{u}_D$ with each of the various Bchl transitions as $\mathbf{u}_A$.

Because of the proximity of the donor and acceptor,[10] the center-to-center distance may provide a poor estimate of the

TABLE 4: Values of the Separation, Orientation Factor (k_F), and Calculated Couplings between the Carotenoid $S_2 \rightarrow S_0$ Transition and Each of the Neighboring Bchl Transitions[a]

Bchl transition	separation (Å)	κ_F	Förster (cm^{-1})	κ_D	density (cm^{-1})
α-B820 Q_x	16.0	−0.36	−19	−0.18	11
α-B820 Q_y	16.0	−0.89	−87	−0.81	−33
β-B820 Q_x	14.2	−1.72	−130	−1.60	−46
β-B820 Q_y	14.2	−0.28	−39	0.11	−45
γ-B820 Q_x	17.1	−1.67	−73	−1.73	−101
γ-B820 Q_y	17.1	1.02	83	0.90	104
B800 Q_x	10.2	−0.18	−37	−0.35	−19
B800 Q_y	10.2	−0.28	−106	−0.31	−45
γ-B800 Q_x	13.2	0.20	19	0.39	35
γ-B800 Q_y	13.2	1.49	260	1.64	173

[a] Separation is the center-to-center distance between the chromophores. Förster is the transition dipole−transition dipole coupling as calculated in section IVC. κ_D is the orientation factor found from the transition density volume calculation. Density is the transition density volume coupling described in section IVC. Species marked α and β refer to the standard Bchl labeling;[10] γ refers to Bchl of the neighboring protomer. Molecular orientations are taken from the crystal structure.[7]

effective separation which determines the coupling. We use the center-to-center distance from the carotenoid to the nearest B820 of 14.2 Å in the following calculations, but note that there is significant uncertainty inherent in this point dipole approach. Values for the transition dipoles are taken to be 13 D for μ_D, which is given for carotenoids in general by Andersson et al.,[50] and 3.3 D for μ_A, which is calculated from Bchl Q_x data in Sauer et al.[51] We take n to be unity as done in previous studies.[47,52]

Use of eq 7 then gives a coupling of 130 cm^{-1}. Combining this with the value of the S_2-Q_x overlap given in Table 3 yields an EET rate of 4.1×10^{12} s^{-1} or 240 fs for $R = 14.2$ Å. Alternatively, we can use the value for k_1 calculated from the carotenoid decay data in section IVA and the S_2-Q_x overlap to work in reverse and give an estimate for the effective carotenoid−Bchl separation. Using a rate of 1.3×10^{13} s^{-1} (78 fs) gives a coupling of 230 cm^{-1} and an effective separation of $R_{eff} = 11.7$ Å.

Though not included in the four-state model of Figure 1, the coupling of the carotenoid $S_2 \rightarrow S_0$ transition to the Bchl $Q_y \leftarrow S_0$ transition can also be determined by using 6.1 D as the magnitude of the $Q_y \leftarrow S_0$ transition dipole.[51] The values of the coupling strengths of the carotenoid $S_2 \rightarrow S_0$ transition to the various transitions of several of the Bchl molecules near to the carotenoid are given in Table 4.

To estimate couplings involving the carotenoid $S_1 \rightarrow S_0$ transition requires more sophisticated techniques. Scholes et al. have examined the S_1-Q_y coupling and found that it is comprised of polarization and Coulombic interactions.[27] In the Förster picture, the deexcitation of the donor molecule interacts resonantly with the transition dipole of the acceptor molecule. In polarization coupling, the deexcitation of a donor molecule interacts nonresonantly with an acceptor molecule by polarizing its electron density. This dipole−induced dipole interaction involves a distance dependence of R^{-5}. The Coulombic term is the combined interaction of the Bchl electric dipole transition moment with both the magnetic dipole (R^{-2}) and the electric quadrupole (R^{-4}) transition moments of the carotenoid. Calculations suggest that exchange interactions are much smaller at all separations[26,27,53] and are considered negligible.

The S_1-Q_y coupling was estimated by Scholes et al.[27] to be 10 cm^{-1} for a carotenoid−Bchl separation of 14.2 Å. With an S_1-Q_y overlap as given in Table 3, this gives a rate of $k_2 = 3.2 \times 10^{10}$ s^{-1} or 32 ps. Earlier in this section, the 78 fs k_1^{-1} value determined from the S_2 emission data was used to calculate an effective carotenoid−Bchl separation of 11.7 Å. Although it is not clear that the same R_{eff} is appropriate for both k_1 and k_2, a coupling of 15 cm^{-1} (given by Scholes et al.[27] for 11.7 Å) results in a rate of $k_2 = 7.1 \times 10^{10}$ s^{-1} or $k_2^{-1} = 14$ ps. Uncertainties in the two values of k_2 are relatively large given lack of a true S_1 emission profile or known S_1 energy in calculation of the spectral overlap and significant uncertainty in the coupling.[27] However, it is reasonable to suggest that S_1-Q_y energy transfer occurs on a picosecond time scale based on these calculations.

The above estimates of electronic coupling depend on our ability to describe changes in the molecular electronic state as a simple scalar or vector located, for example, at the center of the molecule. This approximation works well at separations much larger than the size of the molecules but may not hold in light-harvesting antenna. Furthermore, the changes in electronic density upon excitation may not be uniform enough throughout the molecular volume to be well represented by a single vector. An improved approach is to find the change in electron density throughout the volume of the molecules. The point-by-point interaction of two transition density volumes can then be summed in a straightforward manner. A calculation of this type avoids the need to choose a molecular center and automatically gives the "exact" Coulombic interaction without the need to calculate many terms in the multipole expansion.

A calculation as described above can be carried out in two dimensions following the transition monopole method described by Chang in which a change in electron density is assigned to each atom in the molecule.[54] Nagae et al. extended this technique by including bond transition densities along with atom transition densities.[26] Philipson et al. attempted to take the thickness of chlorophyll π orbitals into account by splitting each transition monopole into two, with half placed above and half below the plane of the molecule.[55] Each of these methods is a significant improvement over the use of a transition dipole; however, none of them are truly three-dimensional.

We have used ab initio methods[56] to calculate the change in electron density throughout a three-dimensional volume (referred to by Gaussian 94 as a "cube") for the carotenoid $S_2 \rightarrow S_0$ transition and the Bchl $Q_x \leftarrow S_0$ and $Q_y \leftarrow S_0$ transitions. These transition density cubes (TDCs) are then interacted to give the "exact" (within the quality of the electron density calculation) Coulombic coupling. We can also calculate appropriate polarizability volumes which should allow estimation of the polarization coupling. A more complete description of this TDC method is given elsewhere.[57] Coupling values calculated in this manner are given in Table 4. In addition, we can recover a transition dipole that best approximates the TDC. These transition dipoles may differ substantially from those used in the Förster calculation, especially in the case of the carotenoid $S_2 \rightarrow S_0$ transition where the twisted structure of the carotenoid makes definition of the transition dipole rather difficult. These TDC-derived transition dipoles are used with eq 8 to give an orientation factor, k_D, from the transition density calculation.

Of primary interest is the magnitude of the difference between the transition dipole−transition dipole (Förster) coupling and the "exact" Coulombic coupling. Generally, the "exact" Coulombic coupling, given by the transition density calculation, is 25−50% smaller in magnitude than the Förster calculation. However, several coupling strengths are very different. We believe this is due to the TDC being poorly represented by the

rather rough estimate of the transition dipole direction or center given earlier or poorly represented by a transition dipole at all.

The difference between the orientation factor as defined for the Förster calculation (k_F) and that found for the transition density calculation (k_D) gives some insight into the accuracy of the point dipole approximation for these molecules. For the coupling of the carotenoid with α-B820 Q_x, β-B820 Q_y, B800 Q_x, and γ-B800 Q_x, k_F is significantly different (a factor of 2 or more) from k_D, implying that the simplistic dipole assumed for the Förster calculation does not well represent the TDC. Also, the transition density calculations for α-B820 Q_x and β-B820 Q_y result in coupling values (density) and orientation factors (k_D) that are opposite in sign. This must result from the three-dimensional nature of the TDC being poorly approximated by its transition dipole.

V. Concluding Remarks

The rates calculated above suggest that path I represents the major contributor of energy transfer from the carotenoid to the Bchl. Assuming that internal conversion from Q_x to Q_y is 100% efficient, an S_2 to Q_x transfer time of 90 fs routes 60% of the excitation placed on the S_2 state to the Q_y state through path I. In contrast, a 14 ps (32 ps) time of the S_1 to Q_y transfer results in 10% (4%) of the excited S_2 population reaching Q_y via path II. In total, our calculations suggest that path I and II account for ∼70% efficient EET from carotenoid to Bchl with the remaining 30% reaching the carotenoid ground state. This efficiency is in good agreement with the 70−75% efficiency determined by steady-state measurements.[33] It should also be noted that three different B820 Bchl are <18 Å away from the carotenoid (see Table 4). Our decay data reflect a transfer time that is the sum of transfer to all of these possible acceptors. From the coupling strengths given in Table 4, it is clear that several transitions should have subpicosecond transfer from S_2, whereas our effective separation (R = 11.7 Å) assumes that only a single B820 molecule is an acceptor.

With regard to the spectral overlap, the broad emission spectrum of the carotenoid makes it extremely well suited to fulfill its role as a donor. Because the broad vibronic line shape of rhodopin glucoside is shared by carotenoids in general, large spectral overlaps should be present in antenna of various carotenoid and Bchl composition. Higher energy (shorter conjugation length) carotenoids, such as spheroidene, are still likely to be efficient donors for both path I and path II transfer. Changes in the energy levels for specific carotenoid and Bchl species in different bacterial systems may tweak both path I and path II transfer efficiencies along with other pathways. In fact, more efficient transfer from carotenoid to Bchl in *Rb. sphaeroides*[24] may be an indication that spheroidene energy levels are properly positioned for efficient energy transfer to both B800 Bchl and B850 Bchl, while *Rps. acidophila* may not efficiently transfer to B800 Bchl.[38]

It should be noted that the calculations of section IVA are based on the four-state model presented in Figure 1, which shows that excitation placed on the carotenoid S_2 state has only two possible routes: internal conversion to S_1 and energy transfer to B820 Bchl Q_x. Using the coupling strengths from Table 4 along with overlaps from Table 3, we estimate that other possible energy acceptors such as neighboring B800 Q_x and Q_y along with B820 Q_y all represent carotenoid to Bchl excitation transfer efficiencies of the order of 1% with transfer times in the few to tens of picoseconds range (hidden by the annihilation kinetics in the B820 emission data of this work). This suggests that a more complete model of the carotenoid−Bchl energy transfer should include several energetic pathways. Unfortunately, to date no experiment that successfully isolates these various pathways has been conducted, and a model that includes all reasonably efficient energetic pathways in this system would be prohibitively complex.

Acknowledgment. We thank Dr. Stephen Bradforth for helpful discussions and Dr. Don Levy for loan of the LBO crystal and the Mira long wave optics set. The work was supported by a grant from the NSF. B.P.K. gratefully acknowledges the support of the ONR through the Department of Defense.

References and Notes

(1) Fleming, G. R.; van Grondelle, R. *Phys. Today* **1994**, *47*, 48−55.
(2) Clayton, R. K. *Photosynthesis: Physical Mechanisms and Chemical Patterns*; Cambridge University Press: New York, 1980.
(3) van Grondelle, R.; Dekker, J. P.; Gillbro, T.; Sundström, V. *Biochim. Biophys. Acta* **1994**, *1187*, 1−65.
(4) Kühlbrandt, W. *Structure* **1995**, *3*, 521−525.
(5) Pullerits, T.; Sundström, V. *Acc. Chem. Res.* **1996**, *29*, 381−389.
(6) Koepke, J.; Hu, X.; Muenke, C.; Schulten, K.; Michel, H. *Structure* **1996**, *4*, 581−597.
(7) McDermott, G.; Prince, S. M.; Freer, A. A.; Hawthornthwaite-Lawless, A. M.; Papiz, M. Z.; Cogdell, R. J.; Isaacs, N. W. *Nature* **1995**, *374*, 517−521.
(8) Hu, X.; Schulten, K. *Phys. Today* **1997**, *50*, 28−34.
(9) Hu, X.; Ritz, T.; Damjanovic, A.; Schulten, K. *J. Phys. Chem. B* **1997**, *101*, 3854−3871.
(10) Freer, A.; Prince, S.; Sauer, K.; Papiz, M.; Hawthornthwaite-Lawless, A.; McDermott, G.; Cogdell, R.; Isaacs, N. *Structure* **1996**, *4*, 449−462.
(11) Frank, H. A.; Cogdell, R. J. *Photochem. Photobiol.* **1996**, *63*, 257−264.
(12) Koyama, Y.; Kuki, M.; Andersson, P. O.; Gillbro, T. *Photochem. Photobiol.* **1996**, *63*, 243−256.
(13) Andersson, P. O.; Gillbro, T. *J. Chem. Phys.* **1995**, *103*, 2509−2519.
(14) Frank, H. A.; Farhoosh, R.; Gebhard, R.; Lugtenburg, J.; Gosztola, D.; Wasielewski, M. R. *Chem. Phys. Lett.* **1993**, *207*, 88−92.
(15) Chynwat, V.; Frank, H. A. *Chem. Phys.* **1995**, *194*, 237−244.
(16) DeCoster, B.; Christensen, R. L.; Gebhard, R.; Lugtenburg, J.; Farhoosh, R.; Frank, H. A. *Biochim. Biophys. Acta* **1992**, *1102*, 107−114.
(17) Shreve, A. P.; Trautman, J. K.; Owens, T. G.; Albrecht, A. C. *Chem. Phys. Lett.* **1990**, *170*, 51−56.
(18) Trautman, J. K.; Shreve, A. P.; Violette, C. A.; Frank, H. A.; Owens, T. G.; Albrecht, C. *Proc. Natl. Acad. Sci. U.S.A.* **1990**, *87*, 215−219.
(19) Trautman, J. K.; Shreve, A. P.; Owens, T. G.; Albrecht, A. C. *Chem. Phys. Lett.* **1990**, *166*, 369−374.
(20) Shreve, A. P.; Trautman, J. K.; Frank, H. A.; Owens, T. G.; Albrecht, A. C. *Biochim. Biophys. Acta* **1991**, *1058*, 280−288.
(21) Ricci, M.; Bradforth, S. E.; Jimenez, R.; Fleming, G. R. *Chem. Phys. Lett.* **1996**, *259*, 381−390.
(22) Andersson, P. O.; Cogdell, R. J.; Gillbro, T. *Chem. Phys.* **1996**, *210*, 195−217.
(23) Förster, T. In *Modern Quantum Chemistry*; Sinanoglu, O., Ed.; Academic Press: New York, 1965; Vol. III, pp 93−137.
(24) Cogdell, R. J.; Frank, H. A. *Biochim. Biophys. Acta* **1987**, *895*, 63−79.
(25) Dexter, D. L. *J. Chem. Phys.* **1953**, *21*, 834−850.
(26) Nagae, H.; Kakitani, T.; Katoh, T.; Mimuro, M. *J. Chem. Phys.* **1993**, *98*, 8012−8023.
(27) Scholes, G. D.; Harcourt, R. D.; Fleming, G. R. *J. Phys. Chem. B* **1997**, *101*, 7302−7312.
(28) Cogdell, R. J.; Durant, I.; Valentine, J.; Lindsay, J. G.; Schmidt, K. *Biochim. Biophys. Acta* **1983**, *722*, 427−435.
(29) Olsen, J. D.; Hunter, C. N. *Photochem. Photobiol.* **1994**, *60*, 521−535.
(30) Fowler, G. J. S.; Visschers, R. W.; Grief, G. G.; van Grondelle, R. *Nature* **1992**, *355*, 848−850.
(31) Mukamel, S.; Rupasov, V. *Chem. Phys. Lett.* **1995**, *242*, 17−26.
(32) Gillbro, T. Personal communication.
(33) Angerhofer, A.; Cogdell, R. J.; Hipkins, M. F. *Biochim. Biophys. Acta* **1986**, *848*, 333−341.
(34) Xie, X.; Du, M.; Mets, L.; Fleming, G. R. In *Time-Resolved Laser Spectroscopy in Biochemistry III*; SPIE: Bellingham, WA, 1992; Vol. 1640, pp 690−706.
(35) Rosenthal, S. J.; Jimenez, R.; Fleming, G. R.; Kumar, P. V.; Maroncelli, M. *J. Mol. Liq.* **1994**, *60*, 25−56.

(36) Bradforth, S. E.; Jimenez, R.; van Mourik, F.; van Grondelle, R.; Fleming, G. R. *J. Phys. Chem.* **1995**, *99*, 16179−16191.

(37) Bradforth, S. E.; Jimenez, R.; Ricci, M.; Dikshit, S. N.; Fleming, G. R. In *Femtochemistry Ultrafast Chemical and Physical Processes in Molecular Systems (Proceedings of Femtochemistry: The Lausanne Conference, 1995)*; Chergui, M., Ed.; World Scientific: River Edge, NJ, 1996; p 427.

(38) Cogdell, R. J. Personal communication.

(39) Zerbetto, F.; Zgierski, M. Z. *J. Chem. Phys.* **1990**, *93*, 1235−1245.

(40) Ganago, A. O.; Parker, E. P.; Laible, P. D.; Albrecht, A. C.; Owens, T. G. *Laser Phys.* **1995**, *5*, 693−698.

(41) Du, M.; Rosenthal, S. J.; Xie, X.; DiMagno, T. J.; Schmidt, M.; Hanson, D. K.; Schiffer, M.; Norris, J. R.; Fleming, G. R. *Proc. Natl. Acad. Sci. U.S.A.* **1992**, *89*, 8517−8521.

(42) Robinson, G. W.; Frosch, R. P. *J. Chem. Phys.* **1962**, *37*, 1962−1973.

(43) Robinson, G. W.; Frosch, R. P. *J. Chem. Phys.* **1963**, *38*, 1187−1203.

(44) Englman, R.; Jortner, J. *Mol. Phys.* **1970**, *18*, 145−164.

(45) Bergström, H.; Sundström, V.; van Grondelle, R.; Gillbro, T.; Cogdell, R. *Biochim. Biophys. Acta* **1988**, *936*, 90−98.

(46) Joo, T.; Jia, Y.; Yu, J.-Y.; Jonas, D. M.; Fleming, G. R. *J. Phys. Chem.* **1996**, *100*, 2399−2409.

(47) Sauer, K.; Cogdell, R. J.; Prince, S. M.; Freer, A.; Isaacs, N. W.; Scheer, H. *Photochem. Photobiol.* **1996**, *64*, 564−576.

(48) Cosgrove, S. A.; Guite, M. A.; Burnell, T. B.; Christensen, R. L. *J. Phys. Chem.* **1990**, *94*, 8118−8124.

(49) Straub, O. *Key to Carotenoids: Lists of Natural Carotenoids*; Birkhäuser: Basel, 1976.

(50) Andersson, P. O.; Gillbro, T.; Ferguson, L.; Cogdell, R. J. *Photochem. Photobiol.* **1991**, *54*, 353−360.

(51) Sauer, K.; Lindsay Smith, J. R.; Schultz, A. J. *J. Am. Chem. Soc.* **1966**, *88*, 2681−2688.

(52) Craig, D. P.; Thirunamachandran, T. *Chem. Phys.* **1989**, *135*, 37−48.

(53) Scholes, G. D.; Harcourt, R. D.; Ghiggino, K. P. *J. Chem. Phys.* **1995**, *102*, 9574−9581.

(54) Chang, J. C. *J. Chem. Phys.* **1977**, *67*, 3901−3909.

(55) Philipson, K. D.; Tsai, S. C.; Sauer, K. *J. Phys. Chem.* **1971**, *75*, 1440−1445.

(56) Frisch, M. J.; Trucks, G. W.; Schlegel, H. B.; Gill, P. M. W.; Johnson, B. G.; Robb, M. A.; Cheeseman, J. R.; Keith, T.; Petersson, G. A.; Montgomery, J. A.; Raghavachari, K.; Al-Laham, M. A.; Zakrzewski, V. G.; Ortiz, J. V.; Foresman, J. B.; Cioslowski, J.; Stefanov, B. B.; Nanayakkara, A.; Challacombe, M.; Peng, C. Y.; Ayala, P. Y.; Chen, W.; Wong, M. W.; Andres, J. L.; Replogle, E. S.; Gomperts, R.; Martin, R. L.; Fox, D. J.; Binkley, J. S.; Defrees, D. J.; Baker, J.; Stewart, J. P.; Head-Gordon, M.; Gonzalez, C.; Pople, J. A. *Gaussian 94, Revision D.4*; Gaussian Inc.: Pittsburgh, PA, 1995.

(57) Krueger, B. P.; Scholes, G. D.; Fleming, G. R. Submitted to *J. Phys. Chem. B.*